Tellus (1993), *45A*, 127–142

Statistical properties of sea ice surface topography in the Baltic Sea

By JOHN E. LEWIS, *McGill University, 805 Sherbrooke St. W., Montreal, Quebec, Canada H3A 2K6*, MATTI LEPPÄRANTA, *Department of Geophysics, University of Helsinki, Fabianinkatu 24 A, SF-00100 Helsinki, Finland*, and HARDY B. GRANBERG, *University of Sherbrooke, Centre d'applications et de recherches en télédétection (CARTEL), Sherbrooke, Quebec, Canada J1K 2R1*

(Manuscript received 27 December 1991; in final form 4 September 1992)

ABSTRACT

The results from helicopter-borne laser profiling of the ice surface in the Baltic Sea for March 1988 are presented. The laser was a PRAM III system with a measurement frequency of 1–4 kHz, a footprint of approximately 20 cm at a flight elevation of 100 m and a single-shot vertical resolution of 12.5 cm. The laser profiles were calibrated to remove aircraft motion and averaged to 1-m intervals which combined to produce an elevation accuracy of 1.8 cm. A total of 51 profiles with varying lengths from 6 to 24 km, in all 662 km, are analyzed. The data were stratified into 5 groups representing different ice fields. The standard deviation of the surface elevations ranged from 7 to 14 cm. The spectrum of surface roughness displayed a red noise form (slope about −1.5) through the wave-lengths 4 to 100 m. Ice ridges were identified using the Rayleigh criterion with a cutoff height of 40 cm. The mean ridge height ranged from 52 to 59 cm, the standard deviation 12 to 20 cm, and the maximum ridge height sampled was 197 cm. The number of ridges was 1.4 to 9.5 km^{-1} for 4 of the groups and up to 17.4 km^{-1} in one group representing an intense shear zone. Ridge heights were exponentially distributed whereas the log-normal distribution provided the best fit for the ridge spacings. Mean ridge height and ridge density were not strongly correlated. The amount of ridged ice was estimated to account for 1 to 18 cm of equivalent ice thickness while based on a crude extrapolation method rubble fields summed up to 2–10 cm. Deformed ice constituted 15–40% of the total ice volume.

1. Introduction

In the northern part of the Baltic Sea ice forms every year. Depending on the location, the average ice season is 3–6 months and the maximum annual ice sheet thickness 10–120 cm. Frequent storms induce mechanical deformation. The deformed ice has fairly rough surface topography and appears as rubble fields and as ice ridges, with thick but long and narrow accumulations of ice blocks. The thickness of ridges is typically 5–15 m and over large areas their mass accounts for, on the average, up to one-third of the total ice mass (Leppäranta and Hakala, 1992). Only 1st-year ice occurs in the Baltic Sea.

Ice ridges are a major obstacle to winter navigation and when in motion cause the largest forces on offshore structures in the Baltic Sea. Consequently, detailed information on the statistical properties of ridges is needed for routine ice mapping and for planning and conducting marine operations. In sea ice geophysics knowledge of ridging characteristics greatly aids the understanding and modeling of large scale ice mechanics. However, for the Baltic Sea quantitative information on this subject is relatively limited.

To increase our understanding of ice ridging in the Baltic Sea, a comprehensive research programme was undertaken in the late 1980s. The work included detailed field investigations of the geometry, internal structure and strength of individual ice ridges (Kankaanpää, 1989; Leppäranta and Hakala, 1992) and the large scale mapping of the ice surface topography, in particular the statistics on the size and spacing of ridges. This paper presents the results of these latter investigations performed with a laser profilometer.

Airborne laser profiling is presently the best method for ice surface topography mapping on a large scale. The first laser profiles over Arctic pack ice were described by Ketchum (1971). He regarded the method suitable for (1) ridge observations, (2) ice type classification, and (3) identification of leads and cracks. By far, the best success with the laser has been obtained in the collection of ridging statistics.

The laser profiling was conducted during the period of 9–13 March 1988 in the Bay of Bothnia, the northern basin of the Baltic Sea. The measurements were made during an extensive sea ice remote sensing phase of BEPERS-88 (Bothnian Experiment in Preparation for ERS-1). This experiment also provided important validation data for Synthetic Aperture Radar (SAR) imagery (Leppäranta and Thompson, 1989). The results have shown promise for the use of SAR in regional mapping of ridging characteristics (Similä et al., 1992). The laser measurement programme and some preliminary results have been presented by Leppäranta et al. (1990). Apart from some earlier shipborne laser profile measurements (Leppäranta and Palosuo, 1981), this is the first substantial series of ice surface profile measurements from the Baltic Sea.

2. The laser data

2.1. *Ice conditions*

The ice season 1987/88 was mild for the Baltic Sea, with conditions that occur about once in 5 years. In early March, the northern ice edge lay slightly south of 63° N whereas its normal location is around 59–60° N (Fig. 1).

Freezing began in the north in mid-November which is normal. By the beginning of December the coastal areas and skerries were ice-covered in the northern Bay of Bothnia but then the growth of the ice cover decreased. Throughout December the drift ice fields were small and relatively thin (less than 10 cm), producing only rafting and jamming in the pack ice. By early January the maximum thickness of undeformed drift ice had increased to 30–40 cm and the first ridges began to appear. Throughout this month, ridging occurred frequently north of 65° N. A deformed ice patch, around 100×50 km, developed in the northern basin during January. The ridges in this section were on the average two months old at the time of laser profiling (Fig. 1).

The ice south of 65° N was thinner than 10 cm in January and no ridging occurred. Freezing of the whole basin first occurred on 28 January which is two weeks later than normal. In February, the ice grew thicker. Easterly winds dominated and ridging was frequent in a 20–30 km wide zone in the western basin extending along a southerly track (Fig. 1). An intense shear zone 2–3 km wide developed along the western fast ice boundary. After the 20th of February, ridging was also reported from the central and southern parts of the Bay of Bothnia. Within the ice field, the thickness increased to 10–30 cm by the beginning of March and the ice movement was substantial.

At the time of the measurements, different ice fields had developed. Ridges were roughly two months old in the northern area, one month in the western zone, and half a month elsewhere. The thickness of the undeformed ice was 10–60 cm. Not much is known about thicknesses of the parent ice which participated in the ridging processes; the few existing observations show 10–30 cm thick ice blocks in the ridge sails (Kankaanpää, 1990). The ice compactness was 90 to 100% in the observation areas.

According to observations, the thickness of snow was 20–40 cm in the northern fast ice zone. In the southern fast ice region, snow thickness was 10–30 cm. There was a substantial amount of a snow-ice in the ice sheet and its thickness increased with each snowfall; the ice/snow interface was very close to the level of the water surface. There are little data on snow thickness in the drift ice area with some observed values indicating a depth of 10–30 cm in the north and 5–15 cm in the south.

2.2. *Measurements*

The ice surface profile measurements were made with a PRAM III laser profiling system which was installed in a helicopter (Jet Ranger). The laser is a gallium-arsenide injection laser diode that generates light pulses at a wavelength of 904 nm with a sampling rate of 1 to 4 kHz. Most of the time the frequency employed was 2 kHz. Since the speed of the helicopter was approximately 40 m/s, the nominal horizontal spacing at 2 kHz sampling rate was 2 cm. The single-shot vertical resolution is 12.5 cm but the elevational accuracy was increased

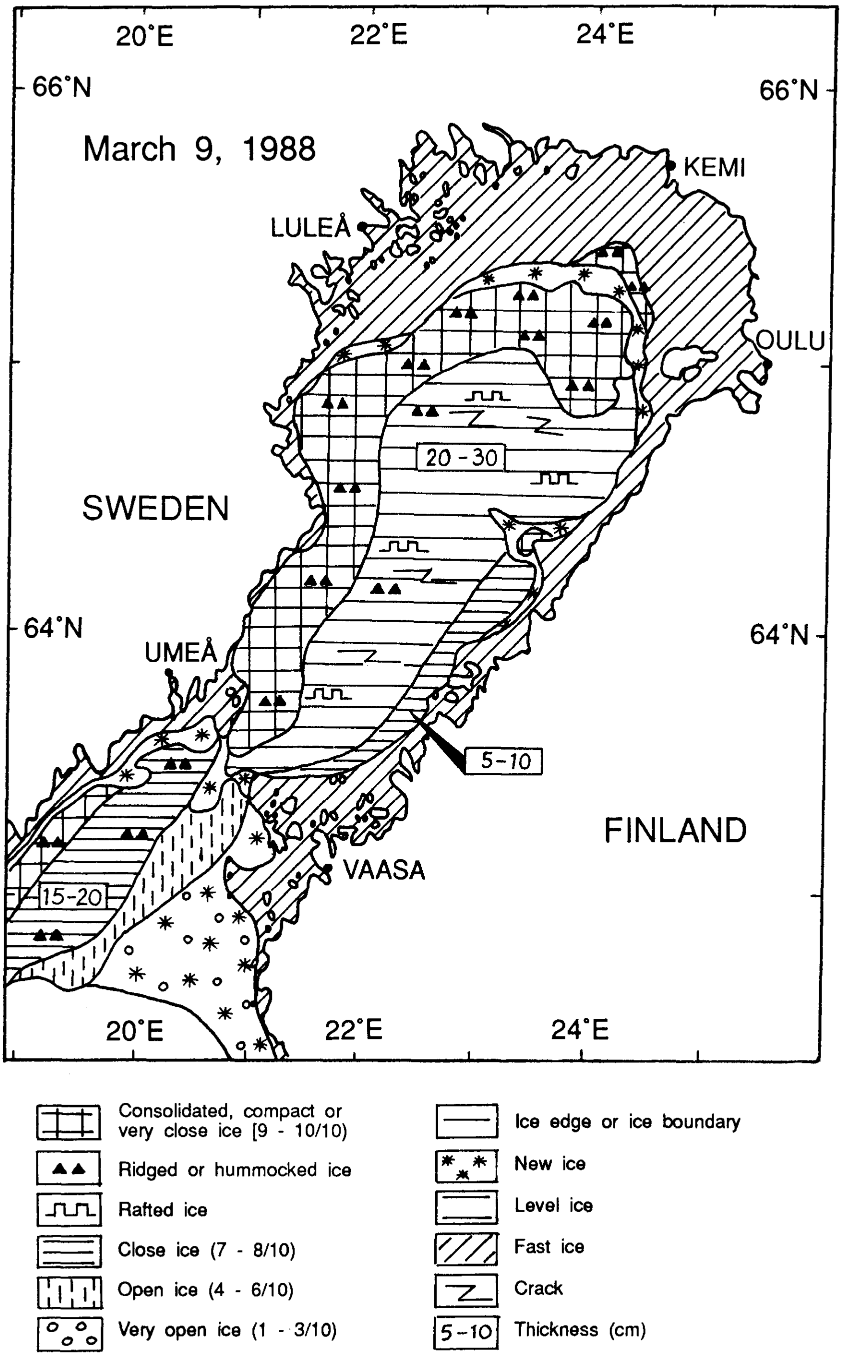

Fig. 1. Map of ice conditions in the Bay of Bothnia, northern Baltic Sea on 9 March 1988.

by averaging several consecutive height determinations. The footprint size of the laser is approximately 20 cm at a flying elevation of 100 m. Along with the digital laser data, accelerometer data, per cent signal return and analogue elevations were recorded. A video camera was operated concurrently with the laser profiler to obtain a visual record of the ice conditions.

The laser profiling covered much of the Bay of Bothnia (Fig. 2). The measurements were made during the period 9 to 13 March 1988 with a total of 61 profiles obtained. Their lengths were from 6 to 24 km depending on the measurement frequency. The sampling strategy was to perform detailed investigations in the western basin in connection with the BEPERS-88 experiment and then obtain a good geographic sample of the ridging characteristics over the whole Bay of Bothnia. Data were collected for 9 to 11 March in the western basin for a total 402 km flown. Also data from a compass rose configuration consisting of four intersecting profiles were collected to study the anisotropy of the ice ridging. On 13 March, a basin-wide measurement series was flown producing 34 12-km profile segements (408 km).

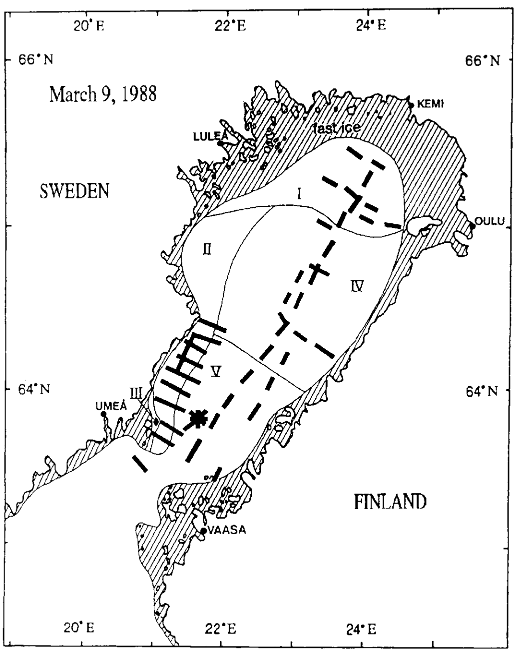

Fig. 2. The locations of the laser profiles and the areal grouping of the data.

The total length of the data set was 810 km. The data and the field experiment are described in detail by Granberg et al. (1988).

Some initial problems in data reduction caused the exclusion of 6 sections. Also 4 profiles from the western area were not considered in the present statistical analysis. A total of 51 profiles covering a length of 662 km were calibrated to yield the surface elevations (Fig. 2).

2.3. Processing of the data

The following procedures were performed in order to convert the raw laser data into profiles of surface elevation of the ice (including the snow).

(1) Dropouts of the laser record occurred when the return signal amplitude fell below approximately 10 per cent. However, by using the analogue (10 Hz) and the % dropout to stretch and match the digital data in regions of dropout, the spatial integrity of the digital trace was preserved. Data dropouts essentially occurred only over water.

(2) Each segment, which consisted of approximately 6×10^5 data values, was checked for wild points. Using a threshold value of 3 m, data greater than this value were excluded. However, none of the data exhibited any outliers.

(3) Since the actual footprint of the laser is 20 cm, the data were block smoothed (averages of 10 consecutive raw data points) to obtain this basic interval. Different spatial increments were then tested on the 20 cm data with a final value of 100 cm chosen for the horizontal spacing. This distance was a compromise between an adequate spatial resolution and the mechanics involved in the calibration procedures. The averaging over the 100 cm interval increases the elevation accuracy to 1.8 cm (divide the single-shot accuracy 12.5 cm by $\sqrt{50}$).

(4) In order to calculate surface ice elevations, the smoothed data must be calibrated by removing the aircraft motion. In removing this motion, we have partially implemented the calibration procedure outlined by Hibler (1972). A high pass non-recursive filter was constructed. An iterative approach was followed by stepping the cutoff wavelength and inspecting the filtered profile and its respective power spectrum. Some form of aircraft motion remained down to 100-m wavelength. This value (100 m) was chosen then as the filter

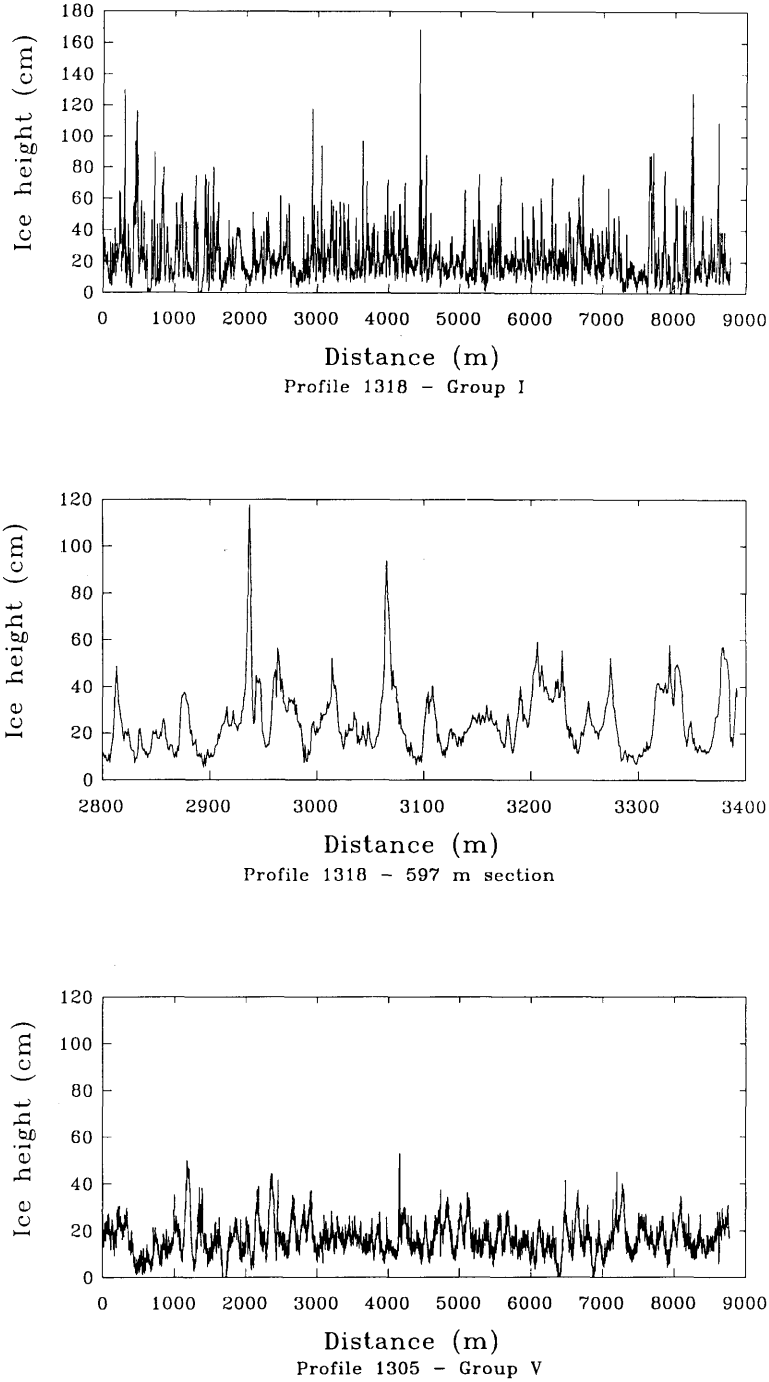

Fig. 3. Surface elevation for two transects in a) northern and c) southern Bay of Bothnia. Fig. 3b) is a 597 m enlarged section of the northern basin transect. The Rayleigh criterion and 40 cm cutoff define individual ridges.

cutoff. From the filtered profile a set of minimum points within a search radius of 10–100 m was obtained. A curve was generated by fitting straight line segments between the minimum points and then a low pass filter applied to this curve. This latter curve was taken to be the aircraft motion which was subtracted from the initial profile to produce the calibrated laser profiles. A helicopter is not the optimum platform for sea ice surface profiling. With a fixed-wing aircraft the cutoff wavelength could be about twice the distance as used in this study (Hibler, 1972).

The filtering procedure caused a loss of data about 1 km from the beginning and end of each profile segment. The total length of the calibrated profiles was reduced to 538 km. Fig. 3 shows surface elevation along two transects representing the northern and southern parts of the basin. The roughness of the surface is clearly decreasing towards the south. The noise in the data (1.8 cm) is well below the amplitude of the signals associated with the ice ridging (see Fig. 3b). With regards to the accuracy in the horizontal, we do not have a complete log of the helicopter velocity; however, we can make some estimates of the spacing error. A general increment for the helicopter velocity fluctuations was ± 4 m/s which would result in a relative error of $\pm 10\%$. As will be shown in Subsection 5.3 the natural variability is much larger for the ridge spacings (see Fig. 8).

2.4. Grouping of the data

The calibrated laser profiles were grouped over the different drift ice areas based on the evolution of the ice conditions during the winter as was described in section 2.1 (Fig. 2). The grouping depresses random sampling effects and gives more reliability in the geographical distribution of the statistical characteristics. The shear zone located at the fast ice boundary in the west was considered as its own group because of its structure being so different from the main pack. The final number of groups decided upon was five and their sum of lengths varied from 30 to 200 km (Table 1; Fig. 2). Also shown in Table 1 are the estimated snow depth data. As the mean snow density was 0.25 g cm^{-3}, these snow thicknesses equal about the amount the undeformed ice could support above the water surface, i.e., the freeboard was approximately zero.

3. Theoretical background

One-dimensional profiles of the ice-covered sea surface are mathematically described by

$$\xi = \xi(x), \tag{1}$$

where ξ is the surface elevation and x is horizontal coordinate. The "surface" is the topmost surface which physically may be water, ice, or snow. The water surface gives a natural zero reference for the surface elevation. Thus, by definition, $\xi = \xi(x)$ is a non-negative one-dimensional spatial series and is equal to max(0, $\xi_i + h_s$) where ξ_i is the ice surface elevation and h_s is snow thickness, and in practical terms ξ equals $\xi_i + h_s$.

Sea ice surface profiles are examined using two types of methods. First, spatial series analysis is performed to study the roughness features. Secondly, ridges are picked from the profile segments and their statistical characteristics are examined.

Table 1. *The grouped profile data*

Group no.	Area	No. profiles	Total length (km)	Thickness of undeformed ice (cm)	Snow depth, mean (cm)	Snow depth, range (cm)
I	northern basin	10	120	30–60	20	10–30
II	western coastal zone	10	200	30–60	15	10–20
III	shear zone	5	30	40–50	10/25*	5–20/5–100*
IV	central basin	13	156	20–30	10	5–15
V	southern basin	13	156	10–20	10	5–15

* Level ice/ridged area.

3.1. Surface roughness

The quantity $\xi(x)$ describes the roughness features of the surface. The average elevation is $\langle \xi \rangle = \langle \xi_i \rangle + \langle h_s \rangle$ (here and below: $\langle \ \rangle$ is the spatial averaging operator). It can be converted to total ice mass if the thickness and density of snow are known. The variance and correlation length of ξ are a simple natural measure of the overall surface roughness characteristics.

Spectral analysis is used to further investigate the distribution of the surface roughness over different wavelengths. Our processed data resolves the wavelengths from 2 m up to the filter cutoff, 100 m. The range is quite limited and excludes the ice block scale roughness of deformed ice as well as the very long wavelength regime where e.g. ice type variations may show up.

3.2. Ridge size

Most of the deformed ice appears as ridges (Fig. 4). The top part of a ridge is called a sail and the laser profile measures its external geometry. Individual sails are taken as selected local maxima of the surface elevation ξ. For the ridge "picking" we have used the Rayleigh criterion with a specified cutoff height following the procedures discussed in Williams et al. (1975) and Wadhams (1981). First, "potential ridges" are selected as the local maxima twice as high as the neighboring minima. Then the "real ridges" are those potential ridges whose height is above the given cutoff height. With the ridges identified (the heights defined as the corresponding local maxima), their statistical characteristics are examined for their distributions of height and spacing.

It is clear that the amount of ridging obtained from the data is sensitive to the choice of the cutoff height. There is no physical criterion to indicate what the cutoff height should be but a proper choice is dictated by two external factors. First, this height must be well above the noise level of the measurement system and, second, the ridges should not be mixed with snow drifts. In the present (smoothed) data, the noise level is very small; therefore, only the elimination of the snow drifts is a concern. An independent verification method for a chosen cutoff height could be aerial photography or just simple visual counts of ridges. This information was not available from the BEPERS experiment.

The probability density of the sail height is expressed in general form as $p = p(h; h_0, \Theta)$ where h_0 is the cutoff height and Θ describes the set of other parameters of the distribution. The first distribution for sail heights, presented by Hibler et al. (1972), assumed that the probability density is proportional to $\exp(-h^2)$. The present understanding, however, usually states that the height distribution is the ordinary exponential distribution, i.e.,

$$p(h; h_0, \lambda) = \lambda \exp[-\lambda(h - h_0)], \qquad h > h_0, \quad (2)$$

where λ is the distribution shape parameter. The mean height is simply $h_0 + \lambda^{-1}$ and standard deviation λ^{-1}. This distribution was first proposed by Wadhams (1980) for Arctic profiles and worked well for Baltic Sea data (Leppäranta, 1981). It has also produced good results in the Antarctic (Weeks et al., 1989; Granberg and Leppäranta, 1990).

The statistical background of the height distribution is based on a certain random hypothesis concerning the probabilities of the different height arrangements (see Hibler et al., 1972). The distribution (2) comes from assuming that all height

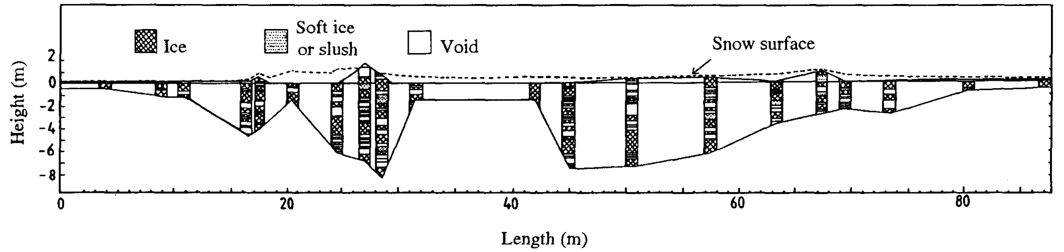

Fig. 4. Cross-section of ridged ice field in March 1988, the Bay of Bothnia western coastal zone (Kankaanpää, 1990). The solid line has been extrapolated between the bore hole measurements.

arrangements yielding the same total sum are equally probable. Such hypothesis, however, has no clear physical background. A heuristic motivation of the exponentiality is a temporal Poisson process for the birth of new ridges in the background. A physical limitation of growth is the existence of a limiting ridge size. If a ridge is allowed to continue growing there exists a limiting vertical size after which the ridge may grow only laterally (Parmerter and Coon, 1972). This size depends on the thickness of the parent ice sheet. Very few ridges ever grow to the limiting size; therefore, these limiting forms are rarely detected in the observed distributions.

3.3. Ridge spacing

The general form of the spacing distribution is $p = p(s; h_0, \Psi)$, where Ψ is the set of parameters in addition to the cutoff height h_0. The inverse mean ridge spacing is called the ridge density, equal to the mean number of ridges per length. The ridge spacing distribution also has usually been taken as exponential which was first presented by Hibler et al. (1972),

$$p(s; h_0, \mu) = \mu \exp(-\mu s), \qquad h > h_0, \tag{3}$$

where $\mu = \mu(h_0)$ is the distribution shape parameter. The mean spacing is simply μ^{-1}. Wadhams and Davy (1986) obtained an even better fit with the log-normal distribution

$$\begin{aligned} p(s; h_0, \theta, \mu, \sigma^2) &= 1/[(s-\theta)\,\sigma\sqrt{2\pi}] \\ &\times \exp\{-[\log(s-\theta)-\mu]^2/2\sigma^2\}, \\ & s > \theta, \end{aligned} \tag{4}$$

where θ is a shift parameter and μ and σ^2 are the mean and variance of the normally distributed $\log(s-\theta)$. The unit is specified here up to an arbitrary scaling factor; if one takes s in meters, then $\exp\{\ \}$ will also be in meters. The parameters θ, μ and σ^2 depend on h_0. The mean spacing is $\theta + \exp(\mu + \sigma^2/2)$ and the modal value is $\theta + \exp(\mu - \sigma^2/2)$. The shift parameter θ defines the minimum spacing between ridges; for ridge sails this minimum is only a few meters and therefore θ may be ignored, i.e., $\theta = 0$.

The spacing distribution is derived from a statistical randomness argument. Hibler et al. (1972) considered the occurrence of ridges (in space) as a Poisson process. More generally, consider the process of randomly splitting a line of fixed length into smaller pieces. If the pieces break with a probability proportional to their size, the exponential distribution results; if the probability is independent of size then the log-normal distribution is obtained. These spacing distributions, therefore, have a sound statistical-physical background. The log-normal distribution has been found to fit with ice floe size distributions very well (Lensu, 1989).

With regard to the two-dimensional aspects of spacing, deviations from isotropy occur as one would expect (e.g., Mock et al., 1972; Leppäranta and Palosuo, 1983). However, the isotropy has so far been the main working hypothesis. It leads simply from one to two dimensions through

$$L/A = \tfrac{1}{2}\pi\langle s\rangle^{-1}, \tag{5}$$

where L is the total length of ridges in horizontal area A and $\langle s\rangle$ is the mean ridge spacing. For anisotropic cases this equation has been found reasonable when using the directionally averaged ridge density parameter.

3.4. Ridging volume and intensity

The observed ridge sails can be used to estimate the total volume of ridged ice. Sail cross-sections can be idealized as triangles with the base at the water surface level (see Fig. 4). The geometry is determined by the ridge height h and slope angle ϕ. The cross-sectional area of a sail is then $S = h^2 \cot \phi$. A representative slope angle is 25° for the Baltic Sea (Kankaanpää, 1989). There is a weak correlation between the slope angle and ridge height but for the volume estimation it is reasonable to treat the angle as constant. The total cross-section of a ridge is obtained using Archimedes' principle:

$$S_R = \kappa h^2 \cot \phi, \tag{6}$$

where the coefficient κ depends on the ridge porosity and ice block density. For the Baltic Sea, the value of κ is 8 (Leppäranta and Hakala, 1992).

The ridge spacing and size distributions can be combined to form a measure of ridging intensity. Two natural measures arise:

$$R_1 = \langle h\rangle\langle s\rangle^{-1}, \qquad R_2 = \langle h^2\rangle\langle s\rangle^{-1}. \tag{7}$$

The first one is dimensionless and describes the sum of ridge heights per unit length; it is also proportional to the aerodynamic form drag of ridges (Arya, 1973). The second one has the dimension of length and is proportional to the mean thickness of ridged ice H_R: from eqs. (5–7) we have

$$H_R = \tfrac{1}{2}\pi\kappa \cot \phi R_2 \tag{8}$$

3.5. Rubble fields

All the mechanically deformed ice does not appear as ridged ice but in places irregular rubble fields are found. Their thickness is less than that of ridges but greater than that of undeformed level ice; they are not detectable from the present laser data. The existence of rubble fields is well known to icebreaker captains who consider them a nuisance because they are easily hidden beneath a snow cover. Not much direct measurement data exist about the spatial distribution of the thickness of rubble. Results in Leppäranta (1981) give some support to a possibility to extrapolate the rubble volume from ridge data as shown below.

Assume that data analysis has produced reasonable theoretical forms to the distributions of ridge height and spacing. The next step is to extrapolate these distributions to zero cutoff and take the pair

$$\lim_{h_0' \to 0} [p(h; h_0', \Theta), p(s, h_0', \Psi) \,|h < h_0], \tag{9}$$

as representing the rubble volume; the notation $|h < h_0$ stands for the conditional distribution, i.e., the lower tail of the limit distribution pair. A wild assumption is made that the volume of rubble becomes represented by the imagined "reference ridges" $h < h_0$. The volume of rubble is then directly obtained from the limit distributions, using also eq. (6), by integration:

$$H_r = \langle S_R \rangle \langle s \rangle^{-1} \,|h < h_0. \tag{10}$$

To extrapolate for the volume of rubble this way is a bit vague and this question needs field data for verification. Knowing the volume of rubble is enough for ice budget calculations but it would be desirable to decompose the volume into mean thickness and aerial concentration. This could be accomplished by establishing an equation for the thickness distribution of rubble.

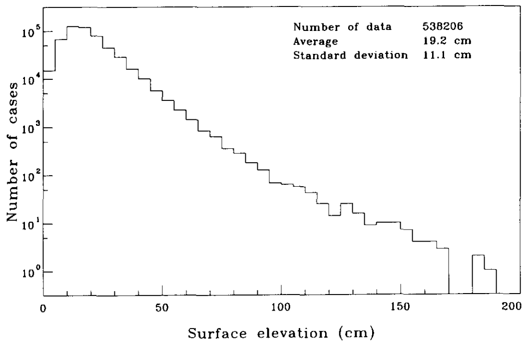

Fig. 5. Histogram for all surface elevation data. Bin size is 5 cm.

4. Results: the surface roughness

The histogram of all the recorded altitudes is shown in Fig. 5. The lower values of distribution describe the snow thickness variations while the ridges are included in the right hand tail of the distribution. The mode of the distribution is located at 10–20 cm whereas the overall average is approximately 19 cm. The probability density falls off smoothly showing no separation between deformed ice and snow drifts. However, the slope becomes more gentle in the upper part of the histogram which may be a characteristic of ridged ice fields. The 90 percentile starts at about 33 cm and 95 percentile at 40 cm.

Table 2 shows the surface elevation statistics for the five data groups. On average, the surface elevation was 16–22 cm above the water level. This was mainly due to the snow cover which produced a freeboard of the ice that was close to zero (see Subsection 2.4). These snow values are a little larger than the estimated average snow thicknesses in Table 1, in particular, for groups IV and V. A small

Table 2. *Basic statistics of the surface elevation*

Group no.	Average (cm)	S.D. (cm)	Max (cm)	Correlation length (m)
I	19.6	11.9	190	43
II	22.3	12.7	183	38
III	21.4	14.1	197	53
IV	17.5	9.2	148	49
V	16.0	7.5	107	49

Zero coincides approximately with the water surface.

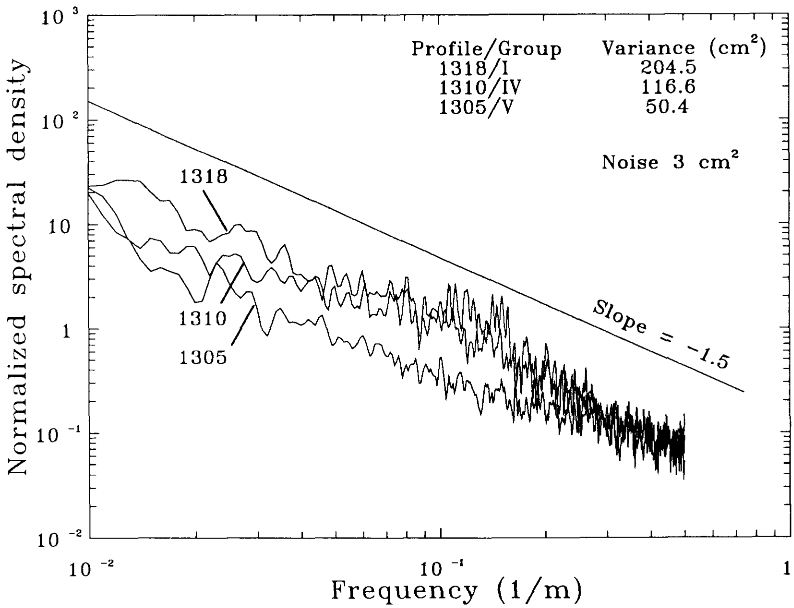

Fig. 6. The spatial spectra of surface elevation for three profiles which represent separate ice groups. The spectral densities have been scaled with the total variance.

bias may exist for the values shown in Table 2. The reason for this is not known. However, two possibilities are: (1) there are substantial along-ridge recordings in the laser data or (2) the results of the filtering procedure (see Subsection 2.3) do not represent the water surface level accurately enough. The standard deviation of the surface elevation was 7–14 cm increasing westward and northward, mainly due to the snow thickness variations which increased with the age of ice.

The largest elevation values, up to 197 cm, are undoubtedly due to ice ridges. The present maximum is still far from the record of 350 cm in the Baltic Sea (Palosuo, 1975). The individual maxima within the 5 groups are more than ten times the standard deviation above the mean. This reflects the dual nature of the data; that is, the spatially dominant and slowly varying snow-covered ice surface with occasional high peaks appearing.

The spectra of 3 ice profiles, one from groups I, IV and V, are shown in Fig. 6. The low wavenumber cutoff is due to the filtering of the helicopter altitude variations which probably also removed some of the surface roughness. The noise level of the laser data which was discussed in section 2 is 3 cm^2. At high wavenumbers the spectra reach the noise level at about 0.25 m^{-1}. Through 0.01 to 0.25 m^{-1} (wavelenghts 4 to 100 m) the spectra are all red, and within these same limits, the variance level increases progressively towards the north indicating an increasing ice roughness. No distinct peaks or shape changes are found in the spectra. A visual power law estimate produced an exponent of -1.5 for the spectral density slopes. Compared with the smoothest profile from group V, the two more deformed profiles show signs of variance increase between 0.03 to 0.2 m^{-1}. This is likely a feature of ridged ice.

5. Results: nature of the ridges

5.1. General

The laser provides a measure of the height of ridge sails which are presumed to have triangular cross-sections (see Fig. 4). As the laser measurements are averages over $\Delta x = 100$ cm lengths and cross the ridge at an angle of β with respect to perpendicular direction, it produces sail height reduced by Δh so that

$$\tfrac{1}{4} \tan \phi' \, \Delta x \leqslant \Delta h \leqslant \tfrac{1}{2} \tan \phi' \, \Delta x, \quad (11a)$$

$$\tan \phi' = \cos \beta \tan \phi, \quad (11b)$$

Table 3. *The basic ridge statistics*

Group No. and No. of profiles		Total length (km)	Height average (cm)	Height S.D. (cm)	Ridge density (km^{-1})
I	$N = 10$	120 (90.2)	58.2	20.2	5.7
II	$N = 10$	200 (185.1)	57.3	17.9	9.5
III	$N = 5$	30 (18.0)	58.8	15.4	17.4
IV	$N = 13$	156 (119.6)	54.3	17.1	2.0
V	$N = 13$	156 (125.4)	52.3	11.6	1.4

Cutoff height is 40 cm. The numbers in parenthesis for the column of total length represent the length after filtering the data.

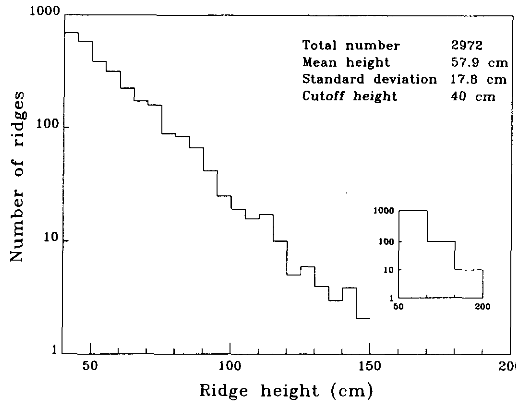

Fig. 7. Ridge height histogram. Ridge data from all five groups are included.

where ϕ' is the sail slope along the laser track. Averaging then over β and the interval in eq. (11a) gives the average reduction of

$$\langle \Delta h \rangle = \tfrac{3}{4}\pi \, \Delta x \tan \phi. \tag{12}$$

With $\phi = 25°$ and $\Delta x = 100$ cm this equation gives $\langle \Delta h \rangle = 11$ cm and from eq. (11a), the range is 0–23 cm. Consequently, the ridge height statistics obtained from the laser data have an average bias of about 10 cm downward. This correction, however, has not been made. The results are correct in the sense that the data represent average elevations over 100 cm intervals and not, e.g., the very tops of ridge sails.

The basic ridge statistics are shown in Table 3. There is a progression westward and northward in the intensity of the ridging. The ridge density ranges from 1.4 to 9.5 km^{-1} except for group III, the shear zone, where the ridges increased to 17.4 km^{-1}. In contrast, the mean ridge height does not vary spatially. It falls in a narrow range, 52 to 59 cm or 12 to 19 cm above the cutoff height. The standard deviation of ridge height shows similar variability as the ridge means with values from 12 to 20 cm. A series of factors such as forcing mechanisms, basin configuration and ice thickness seem to combine to reduce the variability. It is clear that the variations in ridging intensity are mainly due to variations in ridge density and not extensively to ridge height.

5.2. *Ridge heights*

The overall ridge height histogram is plotted in a semi-logarithmic form on Fig. 7 with a 40-cm cutoff value. The histogram is similar to the ridge distributions obtained in the Arctic (Hibler et al., 1972; Hibler et al., 1974; Wadhams, 1981) with clearly a linear slope as expected for the exponential distribution. The Hibler et al. (1972) distribution (see Eq. 4) would decrease quadratically which is evidently too steep when compared to our ridge data.

The form of the observed distribution was tested quantitatively against the exponential distribution. The fitting procedure produced a correlation coefficient of 0.99. The observed vs theoretical distribution passed the Kolmogorov-Smirnov test at the 1% level of significance. For comparison, the gamma and the Weibull distributions were tested but the fits were not as good as with the exponential distribution. It is interesting that the generalization of the exponential distribution to the whole gamma family could not improve the fit. Overall, the Baltic Sea ridge heights confirm very well to the exponential distribution.

One concern with the use of a statistical model is the assessment of the extreme ridge heights. The exponential distribution managed quite well for these conditions (Table 4).

As indicated previously, ridge heights greater than 200 cm are rare which is to be expected since the highest sail height (of floating ridges) ever recorded in the Baltic was 350 cm. However, because of their importance to shipping, the statistics of large ridges have significant practical interest. The tail of a general exponential distribution must be used with extreme care. Therefore, the use of an extreme value distribution was, also, examined. We have applied an extreme value

Table 4. *Observed and predicted tail of the ridge height distribution*

Height (cm)	No. of higher ridges observed	theoretical
100	96	102.1
150	9	6.2
200	≈1 (max = 197)	0.4

(Fisher-Tippet Type I) distribution to the maximum ridge height for each of the 51 ice profiles. There appears to be a good fit with a minor overprediction of 19 cm for the highest ridge height. This value also produced the greatest deviation between the predicted vs observed for the extreme value distribution. The overprediction of ridges in this range of the distribution may be somewhat beneficial for planning decisions but it might add some concern in establishing more confident prediction at the tail of the distributions for other purposes. More data are needed to determine the most appropriate distribution for these ridge heights.

5.3. *Ridge spacings*

The overall spacing distribution is shown in Fig. 8. For illustrative purposes the distribution is shown on both a semi-log and a log-log plot. In the former plot the exponential distribution appears as a straight line whereas in the latter plot the log-normal case is parabolic. Visual inspection suggests that the log-normal gives a better fit. Also in quantitative terms, the log-normal distribution represented the observed data best statistically. Fig. 9 shows that the log-normal distribution passes the Kolmogorov-Smirnov test at the 95% significance level. At this significance level, the hypotheses was rejected that the data are represented by the exponential or gamma distributions. The mean of the best-fit log-normal distribution (121 m) was slightly less than the observed mean (156 m) whereas the modes were close to the observed (10–20 m class, best fit case 16 m).

The exponential distribution clearly underestimates both the short and the long spacings between the ridges. This means that the simple Poisson process does not describe the spacing of ridges very well. In fact, a modified Poisson process would be more representative where the prob-

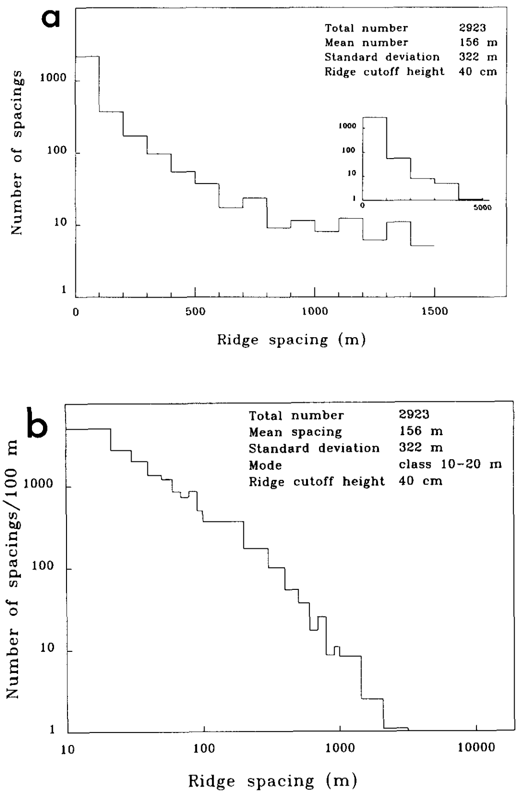

Fig. 8. Ridge spacing histogram for all data: (a) semi-log plot, (b) log-log plot. Bin size for (a) is 100 m and for (b) is decade variable (10 m, 100 m, 1000 m).

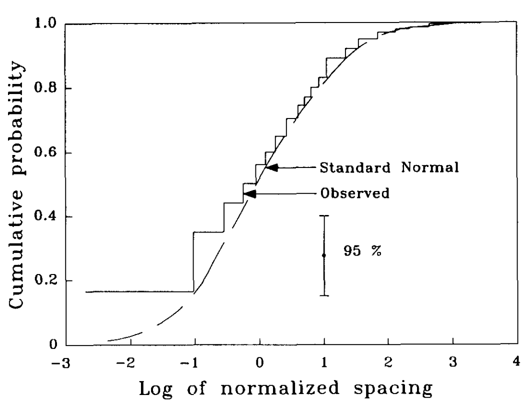

Fig. 9. Cumulative probabilities of the normalized log spacing log $(s - \mu)/\sigma$ and the theoretical standard normal distribution; the 95% mark shows the Kolmogorov-Smirnov test value.

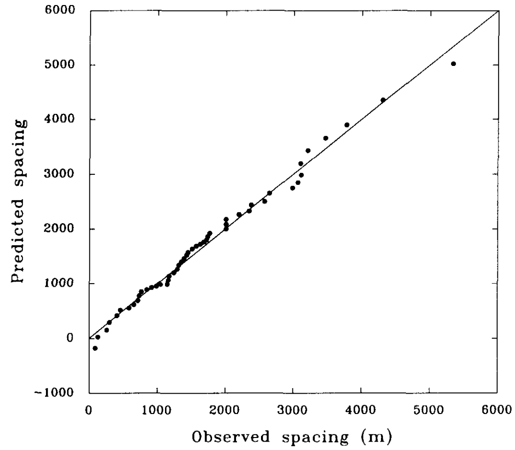

Fig. 10. The histogram of the maximum spacings for the individual profile segments fitted to the Fisher-Tippet type I distribution.

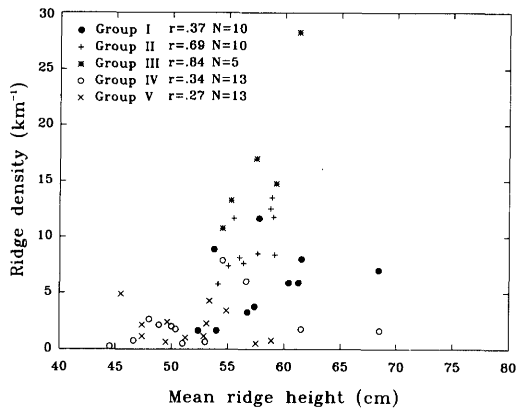

Fig. 11. The joint distribution of the mean ridge height and ridge density for the individual profiles. A different symbol is used to indicate each one of the five ice groups.

ability of finding a new ridge would be increased for small spacings and decreased for large spacings. The log-normal case acts in an opposite way. There is a slight tendency to over predict the tails. However, as shown by the quantitative tests, the log-normal distribution is much closer to the observed data than the exponential case. In physical terms, this suggests that new ridges are initiated in ice floes for which the probability is almost independent of the floe size (see Subsection 3.3).

To provide further description Fig. 10 shows the series of maximum ridge spacing for each of the profiles compared to the extreme value distribution (Fisher-Tippet Type I). This distribution seems to provide a remarkably good characterization of the maximum spacings.

5.4. *Height-spacing relationship*

The mean height and ridge density for all the individual segments are plotted in Fig. 11. The overall correlation coefficient is 0.35. (It is interesting to note that ridge density had higher correlation values with mean ice height and standard deviation, 0.73 and 0.80, respectively.) The reason for these latter correlation values being could be the age of the ice. The data in Fig. 11 are shown in a stratified form by geographical grouping I to V. It is evident that the most deformed areas represented by groups II and III display the highest correlation; however, the sample sizes for the individual groups are small precluding any statement on significance. For comparison, good association has been found in the Arctic between these two quantities (Hibler et al., 1972; Wadhams, 1980 and 1981) with the ridge density plotted on the log scale in Wadhams' analyses. The former calculated a correlation of 0.90 for a combined set of 82 observations while the latter had a correlation of 0.78 for a transect of ≈ 1000 km adjacent to the northeast Greenland coast. However, from his aggregated data (Wadhams, 1980: p. 294) based on the mean values for each of the ten segments, we calculated a lower correlation coefficient of 0.56.

The probable reasons for the difference with our data is the age of the ice fields and frequency of ice types. Even an analysis of individual ridge heights and spacings showed no evidence of any statistical association. Thus, for the Baltic Sea, it is hypothesized that mean ridge height and density are essentially independent.

5.5. *Remarks on the statistical description of ice ridging*

In order to describe the ridging properly, one needs at least three parameters: the cutoff height, the mean height and ridge density. These parameters can be used to obtain a ridging intensity measure but the relationship can not be inverted to obtain ridge heights and spacing from ridge intensity. However, the variation of the mean ridge height for the Baltic seems to be quite small and might be considered fixed to within a rough approximation. For a full statistical description, four parameters are needed if spacing is to be included. Ridge spacings for our data are log-normally distributed which has two independent parameters. This means that the ridge density alone is not sufficient to provide all the information for specifying ridge spacings.

The cutoff height may be thought of as a type of free parameter. It would be a distinct advantage if a constant value for the cutoff height could be used when comparing results from various parts and from different experiments in the Baltic Sea. The present data are not extensive enough to propose a value for this reference height. Further experimental data are needed, in particular more visual ground truth data are required. A standard cutoff height, based on our current best estimates for the Baltic, is about half a meter.

6. Total ice volume

The surface elevation profiles can in principle be transformed to total ice mass using the Archimedes' law. However, due to the uncertainties regarding detailed snow thickness variations, the overall elevation is not suitable for this purpose; ridge data provide better estimates.

The ice pack consists of undeformed ice, rubble and ridges. The total mass can be expressed as thickness, i.e., volume per area, through

$$H = h_1 + H_r + H_R \tag{13}$$

where h_1 represents undeformed ice. The ridge portion can be obtained from the measurement data whereas for the rubble the extrapolation method shown in section 3.5 is utilized. The rubble results must be taken basically in qualitative sense.

The exponential distribution of the ridge height gives

$$S_R = \kappa \cot \phi [\langle h \rangle^2 + (\langle h \rangle - h_0)^2], \tag{14a}$$

$$H_r/(H_r + H_R) = \tfrac{1}{2} \exp(-\lambda h_0)[1 + (\langle h \rangle \lambda)^2]. \tag{14b}$$

The results are shown in Table 5. Ridges accounted for 1–18 cm of equivalent ice thickness and rubble 2–10 cm. The proportion of rubble was greater than the proportion of ridges for areas with a low degree of mechanical deformation whereas in more heavily deformed areas ridges became more dominant. The thickness of deformed ice (ridges + rubble) was 15–40 per cent of the total ice thickness. These figures are in general agreement with earlier data from the Baltic Sea (Leppäranta, 1981). It is interesting that the percentage of deformed ice is of the same order of magnitude as in Arctic seas (e.g., Hibler et al., 1974; Wadhams, 1981). Due to uncertainties in the snow thickness variations it would not be realistic to estimate the total ice volume directly from the profile data using the Archimedes' principle.

Table 5. *Composition of ice mass*

Group no.	Undeformed ice	Deformed ice rubble	Deformed ice ridges	all
I	45	4	6	55
II	45	6	9	60
III	45	10	18	73
IV	25	2	2	29
V	15	2	1	18

Unit cm. The rubble estimates are extrapolated from the ridge results.

7. Conclusions

A laser profilometer mounted on a helicopter was used to examine the ice surface roughness and the size/frequency occurrences of ice ridges in the Baltic Sea. The measurements were made during the period of 9–13 March 1988. The winter season was mild with a thickness of undeformed ice of 10–60 cm. A total of 61 profiles, varying in length from 6–24 km, was collected. From these profiles, 51 were selected for the present statistical analysis representing a total profile length of 538 km after calibration.

Earlier observations of sea ice ridging statistics in the Baltic Sea were made from icebreakers during their routine work (Leppäranta and Palosuo, 1981, 1983). These data are probably biased due to the route selections of the ships. The present airborne laser profiles are the first independent observations and should therefore be taken as the basic reference for Baltic Sea ice ridges.

The data were first stratified into 5 groups representing different ice conditions. The length of combined profiles within each group was 30-200 km. The average surface elevation with respect to the water surface level ranged from 16 to 22 cm, the root-mean-square value was 7–14 cm, and the correlation length of the surface was about 50 m. These values mainly reflect the snow cover thickness variations. The surface elevation spectra were red (slope -1.5) for wavelengths from 4 to 100 m.

Ice ridges were identified using the Rayleigh criterion with a 40-cm cutoff height. The mean ridge heights were from 52 to 59 cm, the standard deviation of the ridges from 12 to 20 cm, and the maximum ridge was 197 cm. The mean ridge density ranged from 1.4 to 9.5 km^{-1} in the main ice pack and 17.4 km^{-1} in the shear zone. The distribution of ridge heights both for the entire sample and for each of the individual ice groups was exponential. The log-normal distribution provided the best fit for the ridge spacings. This distribution generally over predicts distances by ≈ 500 m near the upper tail. For both ridge heights and spacings, an extreme value distribution provides a very good example for representing their statistical character.

Ridge heights and spacings showed poor correlation for the Baltic Sea data. A minimum set of three parameters (cutoff height, mean ridge height and ridge density) is needed to describe the ridge intensity; therefore, without an independent estimate of the cutoff height or one other physical parameter, a statistical formulation of ridging is under prescribed. Ridge density is the most important factor in describing ice ridging variability. The volume of mechanically deformed ice was estimated from the data. Ridges accounted for 1–18 cm of equivalent ice thickness.

The proportion of rubble was extrapolated from the ridge distributions indicating that rubble fields accounted for 2–10 cm of equivalent ice thickness. The thickness of deformed ice (ridges and rubble) was 15–40% of the total ice volume.

This work has attempted to fill a gap in our basic knowledge of sea ice geophysics in the Baltic Sea. Also, the statistical results should be useful in analyzing the ice conditions for engineering purposes. More research is needed to describe and understand the ridging phenomenon. This is especially true if we are to obtain a better physical comprehension of the height distribution, the cutoff question, the implication of rubble fields and the two-dimensional structure of ridging.

8. Acknowledgments

We thank Mr. Patrick Cliche of the University of Sherbrooke who operated the laser system in the field. Mr. Lawrence Houston of McGill University aided in the processing of the laser profiles. His work is gratefully acknowledged. The project was funded by the Academy of Finland and by a grant from the National Science and Engineering Research Council of Canada (NSERC) to Dr. John E. Lewis. We also thank Mr. Len LeSchack for the use of the laser profiling equipment.

REFERENCES

Arya, S. P. S. 1973. Contribution of form drag on pressure ridges to the air stress on Arctic ice. *J. Geophys. Res. 78*, 7092–7099.

Granberg, H. B. and Leppäranta, M. 1990. Helicopterborne remote sensing of Antarctic sea ice using a laser profiler, synchronized video and 70 mm camera during FINNARP-89. *Proceedings of the 10th IAHR Ice Symposium*, vol. 3, pp. 313–325. Espoo, Finland.

Granberg, H. B., Cliche, P., Lewis, J. E. and Leppäranta, M. 1988. *BEPERS-88 helicopterborne laser and video profile surveys; a preliminary report and plots of raw data.* CARTEL, University of Sherbrooke, 170 p.

Hibler, W. D. III 1972. Removal of aircraft altitude variation from laser profiles of the Arctic ice pack. *J. Geophys. Res. 77*, 7190–7195.

Hibler, W. D. III, Weeks, W. F. and Mock, S. J. 1972. Statistical aspects of sea-ice ridge distributions. *J. Geophys. Res. 77*, 5954–5970.

Hibler, W. D. III, Mock, S. J. and Tucker, W. B. III 1974. Classification and variation of sea ice ridging in the Western Arctic Basin. *J. Geophys. Res. 79*, 2735–2743.

Kankaanpää, P. 1989. Structure of first-year ridges in the Baltic Sea. *Proceedings of the 10th Conference on Port and Ocean Engineering under Arctic Conditions* (POAC-89), Luleå University of Technology, vol. I, p. 87–102. Luleå, Sweden.

Kankaanpää, P. 1990. Ice ridges. In: *BEPERS-88: R/V Aranda base ice and snow geophysics data report*, pp. 68–75. Internal Report 1990(4). Finnish Institute of Marine Research, Helsinki, Finland.

Ketchum, R. D., Jr. 1971. Airborne laser profiling of the Arctic pack ice. *Remote Sensing of Environment 2*, 41–52.

Lensu, M. 1989. The random breakage of ice. *Proceedings of Regional and Mesoscale Modelling of Ice Covered Oceans*, pp. 92–96. Conference Report

No. 3, Nansen Remote Sensing Center, Bergen, Norway.

Leppäranta, M. 1981. On the structure and mechanics of pack ice in the Bothnian Bay. Finnish Marine Research No. 248, 3–86.

Leppäranta, M. and Hakala, R. 1992. The structure and strength of first-year ice ridges in the Baltic Sea. *Cold Regions Science and Technology 20*, 295–311.

Leppäranta, M. and Palosuo, E. 1981. Studies of sea ice ridging with a shipborne laser profilometer. *Proceedings of the 6th International Conference on Port and Ocean Engineering under Arctic Conditions* (POAC '81), Vol. II, 1031–1038. Quebec, Canada.

Leppäranta, M. and Palosuo, E. 1983. Use of ship's radar to observe two-dimensional ridging characteristics. *Proceedings of the 7th International Conference on Port and Ocean Engineering under Arctic Conditions* (POAC '83), Vol. I, 138–147. Helsinki, Finland.

Leppäranta, M. and Thompson, T. 1989. BEPERS-88: sea ice remote sensing with Synthetic Aperture Radar in the Baltic Sea. Eos, *Trans. Amer. Geophys. Union 70*, 698–699 and 708–709.

Leppäranta, M., Lewis, J. E. and Granberg, H. B. 1990. The occurrence and size of ice ridges in the Baltic Sea. *Proceedings of the 10th IAHR Ice Symposium*, vol. 1, 314–323. Espoo, Finland.

Mock, S. J., Hartwell, A. and Hibler, W. D. III 1972. Spatial aspects of pressure ridge statistics. *J. Geophys. Res. 77*, 5945–5953.

Palosuo, E. 1975. *Formation and structure of ice ridges in the Baltic.* Winter Navigation Research Board, Rep. No. 12. Board of Navigation, Helsinki, Finland.

Parmerter, R. R. and Coon, M. D. 1972. Model for pressure ridge formation in sea ice. *J. Geophys. Res. 77*, 6565–6575.

Similä, M., Leppäranta, M., Granberg, H. B. and Lewis, J. E. 1992. The relationship between SAR imagery and regional sea ice ridging characteristics. *International Journal of Remote Sensing*, in press.

Wadhams, P. 1980. A comparison of sonar and laser profiles along corresponding tracks in the Arctic Ocean. In: *Sea ice processes and models*, edited by R. S. Pritchard, 283–299. University of Washington Press, Seattle.

Wadhams, P. 1981. Sea ice topography of the Arctic Ocean in the region 70 W to 25 E. *Philosophical Transactions of the Royal Society of London*, Ser. 1A, vol. 302, No. 1464, 45–85.

Wadhams, P. and Davy, T. 1986. On the spacing and draft distributions for pressure ridge keels. *J. Geophys. Res. 91*, 10697–10708.

Weeks, W. F., Ackley, S. F. and Govoni, J. 1989. Sea ice ridging in the Ross Sea, Antarctica, as compared with sites in the Arctic. *J. Geophys. Res. 94*, 4984–4988.

Williams, E., Swithinbank, C. W. M. and Robin, G. de Q. 1975. A submarine sonar study of Arctic pack ice. *J. Glaciol. 15*, 349–362.